International Journal of Innovative Computing, Information and Control
Volume **19**, Number **3**, June **2023**

ICIC International ©2023 ISSN 1349-4198
pp. 941–957

ANTI-DISTURBANCE CONTROL OF TILT DUAL-ROTOR AIRCRAFT UNDER WIND DISTURBANCE

Liben Yang*, Yumin Tang and Wenjun Wei

School of Automation and Electrical Engineering
Lanzhou Jiaotong University
No. 88, Anning West Road, Anning District, Lanzhou 730070, P. R. China
12201468@stu.lzjtu.edu.cn; weiwenjun@mail.lzjtu.com
*Corresponding author: lbyang@mail.lzjtu.cn

Received September 2022; revised January 2023

Abstract. *To address the problems of parameter uncertainty and susceptibility to disturbances from the external wind field of tilt dual-rotor aircraft, this paper proposes a control strategy combining the fuzzy adaptive PID and sliding-mode active disturbance rejection. First of all, according to the Newton-Euler method, a dynamic model of the tilt dual-rotor aircraft under the disturbance of the wind field is constructed. The fuzzy adaptive PID control is adopted for the position outer ring, and the online tuning of the controller parameters is realized by combining the fuzzy control and the PID control. The attitude inner ring adopts the sliding-mode active disturbance rejection control, which combines the sliding-mode control and the active disturbance rejection control. The wind disturbance on the aircraft is estimated using the expanded state observer, and by combining the nonlinear error feedback with the sliding-mode control, the wind disturbance is compensated in real time, which can improve the robustness of the system. Then, Lyapunov is used to prove the stability of the closed-loop system. Finally, the model was constructed on the Matlab/Simulink platform, and the comparative simulation experiments were carried out. The simulation results show that our designed controller can not only effectively resist the disturbances from wind in the simulated environment, but can also achieve stable tracking of position, attitude and flight trajectory, hovering in wind field environment and stable flight, which presents strong robustness.*

Keywords: Tilt dual-rotor aircraft, Wind field disturbance, Fuzzy control, Active disturbance rejection control

1. **Introduction.** Due to its advantages of strong mobility and vertical take-off and landing, the aircraft has been widely used in surveying, mapping, aerial photography, search and rescue and other fields [1-3]. Compared with the traditional four-rotor aircraft, the dual-rotor aircraft has less rotors, increased battery capacity and longer endurance, but it has poorer stability. Therefore, it is particularly important to design a controller with strong anti-disturbance ability and strong robustness [4-7].

When the tilt-rotor aircraft performs tasks outdoors, it is extremely susceptible to the external disturbances, especially the disturbance from ambient wind. Therefore, the wind field disturbance should be considered during design of the controller, so as to improve the controller's adaptability to complex environments, thereby improving the control performance of the aircraft [8-10].

The researchers have proposed a variety of anti-disturbance control methods to handle the disturbance to the aircraft caused by the wind field. For example, [11] proposes an offline wind field estimation method, and based on analysis of how the rotor lift force

DOI: 10.24507/ijicic.19.03.941

changes under the windy conditions, a PID controller is designed to maintain the hovering state of the aircraft. However, this PID controller has poor dynamic performances, which requires a long adjustment time and involves a large overshoot, and the parameters cannot adapt to the external disturbance factors. In [12], an adaptive extended Kalman filter is designed to improve the filtering accuracy of aircraft attitude data by adjusting the adaptive factor of noise in real time, and the data is fed back to the PID position controller for anti-wind disturbance control of the aircraft. However, this method involves a high computational overhead, which will affect its real-time performances. In [13], the sliding-mode control approach is designed to suppress the influence of the wind field on the four-rotor aircraft, and back-stepping control is employed to design a stabilization control term. In this work, it takes a long time for the sliding-mode control to reach the sliding-mode surface, and the initial chattering is not addressed. [14] designs a bi-power sliding-mode approach law controller based on the state observer, the state observer is introduced to estimate and compensate for the wind disturbances in real time, and the attitude controller is designed by combining the bi-power sliding-mode approach law controller with small chattering and fast responses. However, this method has a slow convergence speed, which actually reduces the transition quality at the sliding-mode approach stage.

The tilt dual-rotor aircraft has the characteristics of poor stability and poor wind resistance. To address these problems and meet the requirements of resistance to wind disturbances and robustness of the aircraft, a mathematical model of the aircraft under the wind field is constructed. By adopting the combined control strategy for the inner and outer rings, with the fuzzy adaptive PID as the position outer ring and the sliding-mode active disturbance rejection control as the attitude inner ring, a nested inner-outer ring control strategy is designed to improve the stability under disturbances from the wind field. Our strategy can realize the position and attitude control, hovering control and flight trajectory tracking control of the dual-rotor aircraft. The effectiveness and robustness of the control system are verified by the simulation experiments.

2. **Modeling of the Tilt Dual-Rotor Aircraft under Wind Disturbance.** The tilt dual-rotor aircraft consists of a t-bar and two motors with propellers that can be tilted by 90 degrees forward, backward, leftward and rightward. The rotor speed is regulated by changing the speed ω_i of 2 motors. The rotation of the two rotors generates the upward thrust F_i, and the two rotors move in opposite directions to offset the reactive torque generated between the rotors. The Euler angles – pitch angle θ, roll angle ϕ and yaw angle ψ – are used to describe the motion states of the aircraft body.

As shown in Figure 1, the motor No. 1 rotates clockwise and the motor No. 2 rotates counterclockwise to establish the body coordinate system $x_b y_b z_b$ and the ground coordinate system $x_e y_e z_e$ of the tilt dual-rotor aircraft. The center of gravity of the aircraft is selected as the origin O_b of the body coordinate system, and the origin O_e of the ground coordinate system has fixed connection with the ground.

To simplify the dynamic model, the following assumptions are made for the aircraft:

1) The fuselage of the aircraft is rigid, and the structure is completely symmetrical;

2) The origin of the aircraft fuselage coordinate system coincides with the mass point;

3) The thrust and resistance are proportional to the square of the rotor speed.

The rotation matrix R between the body coordinate system and the ground coordinate system is

$$R = \begin{bmatrix} c_\psi c_\theta & s_\phi s_\theta c_\psi - s_\psi c_\phi & c_\phi s_\theta c_\psi + s_\psi s_\phi \\ s_\psi c_\theta & s_\phi s_\theta s_\psi + c_\psi c_\phi & c_\phi s_\theta s_\psi - c_\psi s_\phi \\ -s_\theta & s_\phi c_\theta & c_\phi c_\theta \end{bmatrix} \tag{1}$$

where $c_{(\bullet)}, s_{(\bullet)}$ represent $\cos(\bullet)$, $\sin(\bullet)$, respectively.

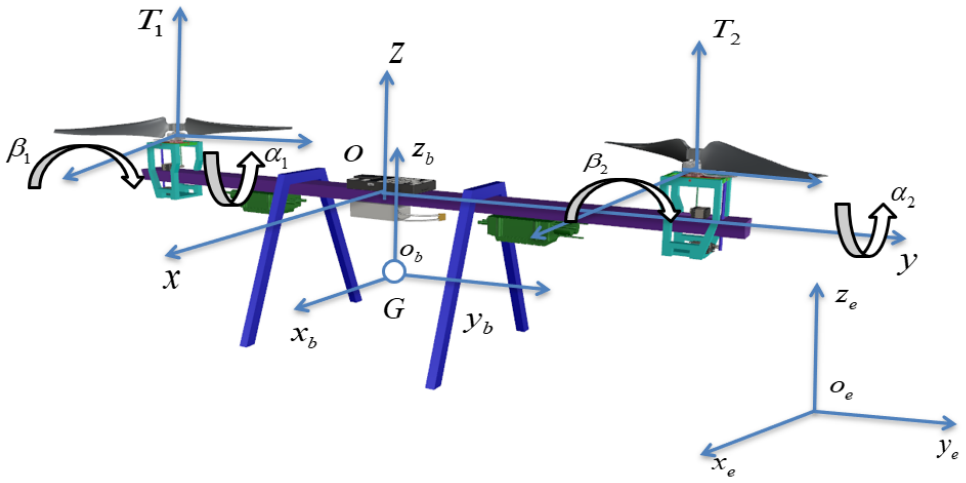

FIGURE 1. Physical model of the tilt dual-rotor aircraft

The rotation matrices $R_x(\beta_i)$ and $R_y(\alpha_i)$ are as shown in Equations (2) and (3). By using the tilt angles (β_i) and (α_i), and the x and y axes, the thrust vector is converted into a force vector applied to the center of gravity G of the body.

$$R_x(\beta_i) = \begin{pmatrix} 1 & 0 & 0 \\ 0 & \cos\beta_i & -\sin\beta_i \\ 0 & \sin\beta_i & \cos\beta_i \end{pmatrix} \tag{2}$$

$$R_y(\alpha_i) = \begin{pmatrix} \cos\alpha_i & 0 & \sin\alpha_i \\ 0 & 1 & 0 \\ -\sin\alpha_i & 0 & \cos\alpha_i \end{pmatrix} \tag{3}$$

2.1. **Aerodynamic analysis.** When there is wind, the aerodynamic analysis of the rotors under the effect of the wind field is shown in Figure 2.

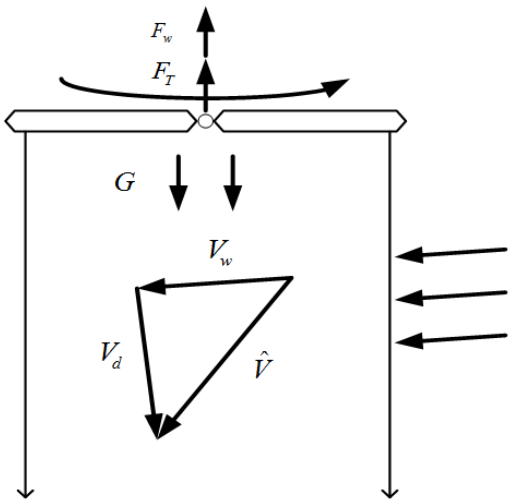

FIGURE 2. Force analysis of rotor

In Figure 2, V_d is the induced velocity of the rotor, V_w is the wind velocity, and $\hat{V}$ is called the total induced velocity, which can be expressed as

$$\hat{V} = V_d + V_w \tag{4}$$

The induced velocity of the rotor V_d is defined as

$$\|V_d\| = \sqrt{\frac{F_T}{2\rho A}} \tag{5}$$

where F_T is the pulling force of the rotor, ρ is the density of the air, and A is the area of the paddle.

According to the rotor slip flow theory, the lift force of the rotor when there is no wind can be expressed as

$$F_{T_0} = 2\rho A v_d^2 \tag{6}$$

where ρ represents the air density and A represents the effective area of the paddle.

Under the effect of the wind field, the total lift force of the rotors can be expressed as

$$F_T = 2\rho\pi R^2 v_d \left|v_d + v_w\right| = 2\rho\pi R^2 v_d \hat{v} \tag{7}$$

2.2. **Dynamic model of tilt dual-rotor aircraft.** When a rigid body with mass m is subjected to the force $F_{tot} \in R_3$ of the body, and the moment $M_{tot} \in R_3$ acting on the center of mass is given by the Newton-Eulerian method, its motion equation in the body coordinate system b and ground coordinate system e can be expressed as

$$\begin{aligned} F_{tot}^e &= m\dot{V}^e + \Omega \otimes mV \\ M_{tot}^b &= J\dot{\Omega} + \Omega \otimes J\Omega \end{aligned} \tag{8}$$

where $V = (\dot{x}, \dot{y}, \dot{z})^T \in R^3$ is the velocity vector of the tilt rotor, and $\otimes$ is the cross product.

The total force F_{tot}^e acting on the center of gravity G is the sum of gravity F_g^e and thrust F_G^e, as shown in Equation (9) [15].

$$F_{tot}^e = F_g^e + F_G^e = (0, 0, mg) + R * F_G^b \tag{9}$$

The direction of the thrust can be changed by tilting the propeller. The thrust T_i $(i = 1, 2)$ generated by the rotor can be expressed by Equation (10), and the total thrust F_G^b can be expressed by Equation (11).

$$T_i = C_T \omega_i^2 \tag{10}$$

$$\begin{aligned} F_G^b &= \left(R_{xy}(\beta, \alpha)_1 T_1 + R_{xy}(\beta, \alpha)_2 T_2\right) e_3 + w_1 \\ &= \begin{pmatrix} \sin\alpha_1 T_1 + \sin\alpha_2 T_2 + w_1 \\ -\sin\beta_1 \cos\alpha_1 T_1 - \sin\beta_2 \cos\alpha_2 T_2 + w_1 \\ \cos\beta_1 \cos\alpha_1 T_1 + \cos\beta_2 \cos\alpha_2 T_2 + w_1 \end{pmatrix} \end{aligned} \tag{11}$$

where w_1 is the influence of wind field disturbance.

Therefore, the translation equation can be represented by Equation (12).

$$\begin{cases} m\ddot{x} = \left(c_\psi c_\theta\right) F_x - \left(s_\phi s_\theta c_\psi - s_\psi c_\phi\right) F_y + \left(c_\phi s_\theta c_\psi + s_\psi s_\phi\right) F_z + w_1 \\ m\ddot{y} = \left(s_\psi c_\theta\right) F_x - \left(s_\phi s_\theta s_\psi + c_\psi c_\phi\right) F_y + \left(c_\phi s_\theta s_\psi - c_\psi s_\phi\right) F_z + w_1 \\ m\ddot{z} = \left(-s_\theta\right) F_x + \left(s_\phi c_\theta\right) F_y + \left(c_\phi c_\theta\right) F_z - mg + w_1 \end{cases} \tag{12}$$

The total moment on the tilt rotors is represented by Equation (13), which is composed of the gyro moment M_{gyro}^b, the resisting moment M_{prop}^b, the thrust moment M_{thrust}^b, the torque caused by wind field M_{wind}^b and the reaction moment M_{react}^b.

$$M_{tot}^b = M_{gyro}^b + M_{thrust}^b + M_{prop}^b + M_{wind}^b - M_{react}^b = [M_x, M_y, M_z]^b \tag{13}$$

The rotation equation can be expressed as Equation (14):

$$\begin{cases} J\ddot{\phi} = \dot{\psi}\dot{\theta}\left(J_y - J_z\right) + M_x^b \\ J\ddot{\theta} = \dot{\phi}\dot{\psi}\left(J_z - J_x\right) + M_y^b \\ J\ddot{\psi} = \dot{\theta}\dot{\phi}\left(J_x - J_y\right) + M_z^b \end{cases} \tag{14}$$

A simplified model is proposed, and the dynamic model is modified into Equation (15):

$$\begin{cases} m\ddot{x} = C_T U_1 \left[\left(c_\psi c_\theta\right)\alpha - \left(s_\phi s_\theta c_\psi - s_\psi c_\phi\right)\beta + \left(c_\phi s_\theta c_\psi + s_\psi s_\phi\right)\right] + w_1 \\ m\ddot{y} = C_T U_1 \left[\left(s_\psi c_\theta\right)\alpha - \left(s_\phi s_\theta s_\psi + c_\psi c_\phi\right)\beta + \left(c_\phi s_\theta s_\psi - c_\psi s_\phi\right)\right] + w_1 \\ m\ddot{z} = C_T U_1 \left[\left(-s_\theta\right)\alpha - \left(s_\phi c_\theta\right)\beta + \left(c_\phi c_\theta\right) - mg\right] + w_1 \\ J_x\ddot{\phi} = \dot{\psi}\dot{\theta}\left(J_y - J_z\right) - l_0 C_T U_2 + \alpha C_Q U_2 - \beta h_0 C_T U_1 + w_2 \\ J_y\ddot{\theta} = \dot{\phi}\dot{\psi}\left(J_z - J_x\right) - \beta C_Q U_2 - \alpha h_0 C_T U_1 + w_3 \\ J_z\ddot{\psi} = \dot{\theta}\dot{\phi}\left(J_x - J_y\right) + l_0 \alpha C_T U_2 + C_Q U_2 + w_4 \end{cases} \tag{15}$$

where J_x, J_y, J_z are the moments of inertia of the axes x, y, z, respectively; l is the distance between the rotor and the aircraft's center of mass; w_2, w_3, w_4 represent the influence of the wind field disturbance.

2.3. **Wind field model.** In this paper, the Dryden atmospheric turbulence model is used, and the simulation of atmospheric turbulence is completed by passing the standard Gaussian white noise sequence through a shaping filter to form a colored noise sequence. The time spectrum function is

$$\begin{cases} \Phi_{w_x}(\omega) = \sigma_x^2 \dfrac{L_x}{\pi v} \dfrac{1}{1 + \left(\frac{L_x}{v}\omega\right)^2} \\ \Phi_{w_y}(\omega) = \sigma_y^2 \dfrac{L_y}{\pi v} \dfrac{1 + 12\left(\frac{L_y}{v}\omega\right)^2}{\left[1 + 4\left(\frac{L_y}{v}\omega\right)^2\right]^2} \\ \Phi_{w_z}(\omega) = \sigma_z^2 \dfrac{L_z}{\pi v} \dfrac{1 + 12\left(\frac{L_z}{v}\omega\right)^2}{\left[1 + 4\left(\frac{L_z}{v}\omega\right)^2\right]^2} \end{cases} \tag{16}$$

where σ_x, σ_y, σ_z represent the turbulence intensities in three directions, L_x, L_y, L_z refer to the turbulence scale in three directions, and v represents the flight speed of the aircraft.

Because of the limited flight height of the dual-rotor aircraft, under low altitude (lower than 1000 feet), the turbulence intensity and turbulence scale can be calculated by Equation (17).

$$\begin{cases} L_u = 2L_v = \dfrac{h}{(0.177 + 0.000823h)^{1.2}} \\ L_w = \dfrac{h}{2} \\ \sigma_u = \dfrac{\sigma_w}{(0.177 + 0.000823h)^{0.4}} \\ \sigma_v = \dfrac{\sigma_u}{(0.177 + 0.000823h)^{0.4}} \\ \sigma_w = 0.1u_{20} \end{cases} \tag{17}$$

where h represents the flight height, and u_{20} represents the wind speed at the height of 6.096 m (20 feet).

When Equation (18) is decomposed and simplified into the first-order form, the fixed frequency filter is

$$\begin{cases} G_u(s) = \dfrac{K_u}{T_u s + 1},\ K_u = \sigma_u \sqrt{\dfrac{L_u}{\pi v}},\ T_u = \dfrac{L_u}{v} \\ G_v(s) = \dfrac{K_v}{T_v s + 1},\ K_v = \sigma_v \sqrt{\dfrac{L_v}{\pi v}},\ T_v = \dfrac{2L_v}{\sqrt{3}v} \\ G_w(s) = \dfrac{K_w}{T_w s + 1},\ K_w = \sigma_w \sqrt{\dfrac{L_w}{\pi v}},\ T_w = \dfrac{2L_w}{\sqrt{3}v} \end{cases} \tag{18}$$

3. **Design of the Tilt Dual-Rotor Aircraft Controller.** Its control system adopts cascade control, with the position subsystem as the outer ring and the attitude subsystem as the inner ring. It is divided into 4 channels: the height channel, the x-θ channel, the y-ϕ channel and the yaw channel ψ. This paper proposes a nested inner-outer ring control strategy to control the aircraft, with the fuzzy adaptive PID control as the outer ring, and with the sliding-mode active disturbance rejection control as the inner ring. The block diagram of the control system is shown in Figure 3.

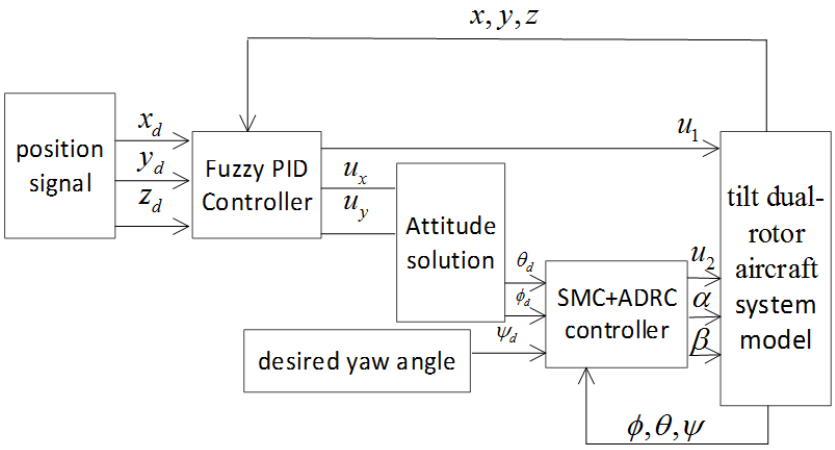

FIGURE 3. Structure diagram of control system

3.1. **Design of the position controller.** The outer ring of the aircraft is a position ring, which contains three independent loops used to control the motions of the aircraft in the three axes of x, y, z, respectively.

3.1.1. *Design of the PID controller.* The position control includes control in the horizontal and vertical directions. The vertical position control is height control. The difference between the actual height z and the expected height z_d is used as the control quantity, and the height control is designed as

$$\ddot{z} = k_{p,z}(z - z_d) + k_{i,z} \int (z - z_d)dt + k_{d,z}(\dot{z} - \dot{z}_d) \tag{19}$$

where $\ddot{z}$ is the target height acceleration parameter. The height control quantity can be obtained as

$$u_z = \left(k_{p,z}(z - z_d) + k_{i,z} \int (z - z_d)dt + k_{d,z}(\dot{z} - \dot{z}_d) \right) \Big/ \cos\phi \cos\theta \tag{20}$$

For the horizontal position control, set (x_d, y_d) as the expected target position in the horizontal direction, compare it with the flight position to obtain the position error, use the position error as the input, and the horizontal position control is

$$\begin{cases} \ddot{x} = k_{p,x}(x - x_d) + k_{i,x} \int (x - x_d)dt + k_{d,x} (\dot{x} - \dot{x}_d) \\ \ddot{y} = k_{p,y}(y - y_d) + k_{i,y} \int (y - y_d)dt + k_{d,y} (\dot{y} - \dot{y}_d) \end{cases} \tag{21}$$

3.1.2. *Design of the fuzzy adaptive PID controller.* Fuzzy control is an automatic control method that adopts the language control rules, which does not need to construct an accurate mathematical model of the controlled object, and its realization does not require abstracting the measured data or expert experience into control rules. The fuzzy adaptive PID system can be divided into the fuzzy inference part and the PID controller. The error e and change in error ec are the input of controller, while the PID parameters as the output. The error e and change in error ec at different moments are fuzzified, and then the designed fuzzy rules are used for defuzzification. Set Kp, Ki and Kd as the controller output values, Kp^*, Ki^* and Kd^* as the basic values of the PID parameters, and ΔKp, ΔKi and ΔKd as the online tuning values of the PID parameters. The calculated values of ΔKp, ΔKi and ΔKd are integrated into the original PID system to establish a new PID control system. The output PID parameter values are the sums of the basic values of the PID parameters and the online setting values of the PID parameters, and their relationships are shown in Equation (22):

$$\begin{cases} Kp = Kp^* + \Delta Kp \\ Ki = Ki^* + \Delta Ki \\ Kd = Kd^* + \Delta Kd \end{cases} \tag{22}$$

The control rule of the fuzzy adaptive PID is

$$u(k) = Kpe(k) + Ki \sum_{i=1}^{n-1} e(k) + Kde_c(k) \tag{23}$$

where $e(k)$ is the control error; $e_c(k)$ is the control change in error; Kp is the proportional coefficient; Ki is the integral coefficient; Kd is the differential coefficient.

3.1.3. *Numerical fuzzification.* The fuzzy subset is determined for the input e and ec, and the fuzzy subset {NB, NM, NS, ZO, PS, PM, PB} can be selected as for the PID control, which are assigned with the variable language of "negative big, negative medium, negative small, zero, positive small, positive medium, positive big". The fuzzy set domain of discourse for e and ec is introduced. After normalization, the domain of discourse is $\{-1, 1\}$, the scale factor is set to 3 by using the empirical method, and the domain of discourse is defined as $\{-3, 3\}$. Similarly, the same fuzzy subset {NB, NM, NS, ZO, PS, PM, PB} can be selected for ΔKp, ΔKi, and ΔKd. For the fuzzy set domain of discourse, $\Delta Kp \in \{-0.3, 0.3\}$, $\Delta Ki \in \{-0.06, 0.06\}$, $\Delta Kd \in \{-0.3, 0.3\}$. According to the membership, the memberships occupied by the input e and ec can be inferred. Considering the coverage, sensitivity and adjustment difficulty of the domain of discourse, the triangular membership functions are selected for all the above fuzzy subsets. The membership function curves are shown in Figure 4.

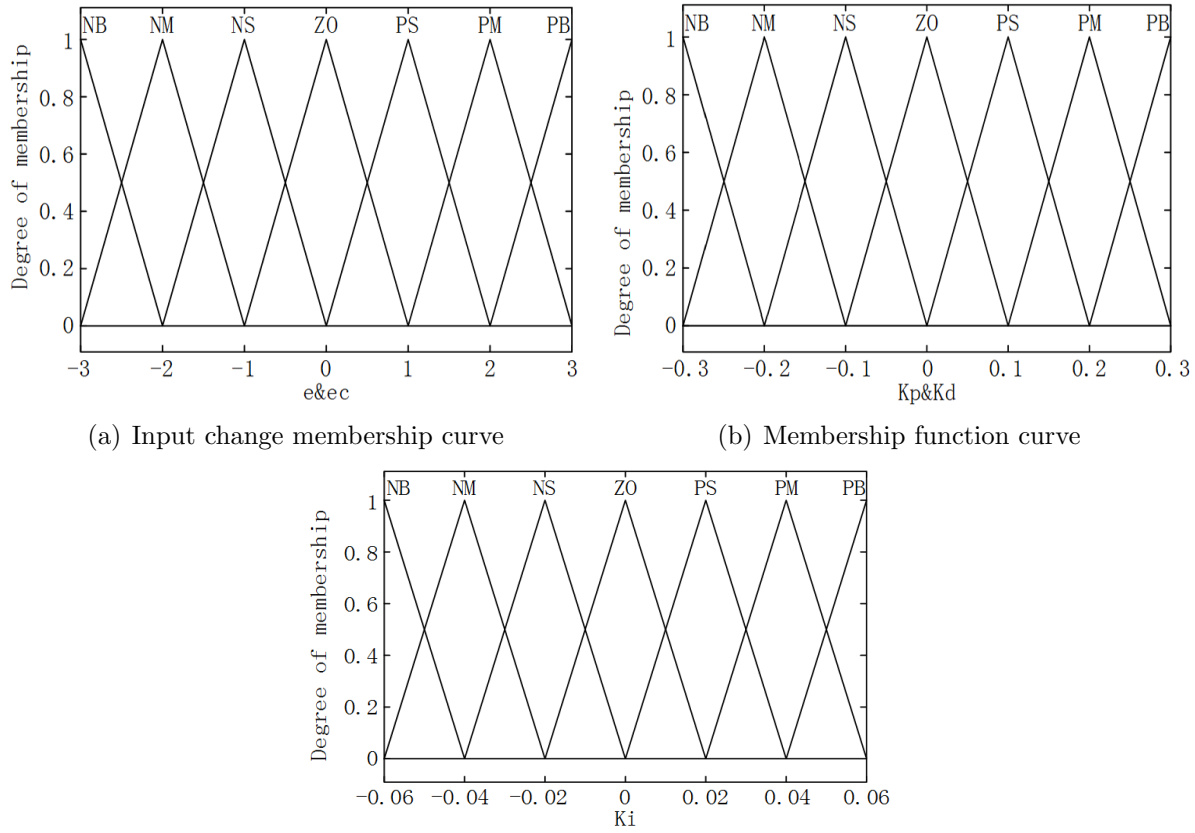

(a) Input change membership curve

(b) Membership function curve

(c) Membership function curve

FIGURE 4. Membership of fuzzy adaptive PID control

3.2. **Design of attitude controller.** The inner ring of the aircraft is the attitude ring. The attitude inner ring adopts the sliding-mode active disturbance rejection control, and the control strategy combining the sliding-mode control and active disturbance rejection control is adopted to control the rotation angles θ, ϕ, ψ of the aircraft around the three axes of x, y, z.

The active disturbance rejection control can estimate and compensate for the internal disturbance and external unknown disturbance to the system in real time, and it consists of three parts of the tracking differentiator (TD), the extended state observer (ESO), and the nonlinear state error feedback (NLSEF). Each channel uses ESO to estimate the wind field disturbance w in real time and compensate for the error caused by the disturbance, so as to realize the decoupling control of the aircraft. In this paper, the model-compensation active disturbance rejection control is used to fully utilize the model information of the aircraft, reduce uncertainty and improve the control performance. As long as z_1, z_2 can well track the aircraft state, $f(z_1, z_2)$ can well track the aircraft, so as to reduce the estimated value $f(x_1, x_2) - f(z_1, z_2)$ of z_3. See Figure 5 for the structure of the controller.

3.2.1. *Tracking differentiator (TD).* In this paper, a third-order tracking differentiator is used to obtain the second-order sliding-mode command signal of the SMC+NLSEF module. The TD controller can be used to arrange the transition between the given signal and the controller, which can not only solve the contradiction between overshoot and fast speed, but also expand the range of error feedback gain and error differential feedback

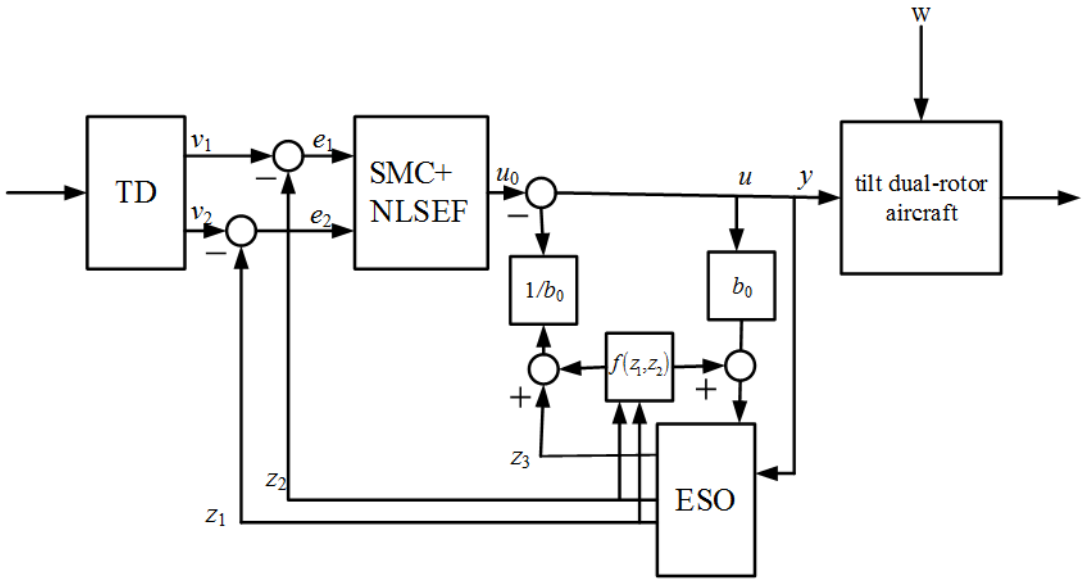

FIGURE 5. Structure of active disturbance rejection control

gain. The expression of the third-order tracking differentiator is

$$\begin{cases} \dot{v}_1 = v_1 \\ \dot{v}_2 = v_2 \\ \dot{v}_3 = v_3 \\ f = (-r(r(r(v_1 - v_0) + 3v_2) + 3v_3)) \end{cases} \tag{24}$$

where r is the rapid factor of the tracking differentiator; the r parameter is adjustable, which determines the tracking speed of the output signal, and the larger r is, the shorter the transition process.

3.2.2. *Combination of the sliding-mode control and nonlinear state error feedback (SMC +NLSEF).* The nonlinear state error feedback is used to generate an initial control variable and eliminate the difference between the error signal of the tracking differentiator and the disturbance estimated by the extended state observer. The input is the difference between the transition signal and differential signal output by the TD module and the z_1 and z_2 output by the ESO module, and the current feedback control quantity u_0 of the system can be obtained. The final control quantity u is determined according to the virtual control quantity u_0 plus the compensation value estimated based on the total disturbance. The expression is

$$\begin{cases} e_1 = v_1 - z_1 \\ e_2 = v_2 - z_2 \\ u_0 = k_1 fal\left(e_1, a_1, \delta_0\right) + k_2 fal\left(e_2, a_2, \delta_0\right) \\ u = u_0 - \dfrac{z_3}{b} \end{cases} \tag{25}$$

where k_1 and k_2 affect the response speed of the system: increasing k_1, the system response speed will become faster; increasing k_2, the oscillation and overshoot can be suppressed.

The sliding-mode control is introduced into the nonlinear state error feedback for optimization, so as to improve the parameter tuning and the control performance of the controller.

To derive the above equation, we have

$$\begin{cases} \dot{e}_1 = e_2 = v_2 - z_2 \\ \dot{e}_2 = bu_0 \\ u = u_0 - \dfrac{f}{b} \end{cases} \tag{26}$$

where f is disturbance.

The linear sliding surface is adopted during design of the set control quantity u_0, and the expression is

$$s = ce_1 + e_2 \tag{27}$$

c is the sliding surface parameter, which is bigger than 0. Take the derivative of c, and we have

$$\dot{s} = ce_2 + \dot{e}_2 \tag{28}$$

Using exponential approach to make the state variables in the control law close to the sliding surface, we have

$$-ksign(s) - qs = ce_2 + bu_0 \tag{29}$$

$$u_0 = \frac{-ksign(s) - qs - ce_2}{b} \tag{30}$$

where k, q, c are the exponential approach coefficients, all of which are bigger than 0.

To prove the stability of the sliding-mode set control quantity, the Lyapunov method is employed for stability analysis.

$$s * \dot{s} = [-ksign(s) - qs]s = -k|s|^2 - qs^2 \leq 0 \tag{31}$$

Then, the system stability is proved.

3.2.3. *Extended state observer (ESO).* The extended state observer (ESO) is used to estimate the internal and external disturbances to the system, its input is the system output y and the NLSEF output u, and its output is z_1, z_2, z_3. Its expression is

$$\begin{cases} e = z_1 - y \\ \dot{z}_1 = z_2 - \beta_1 e \\ \dot{z}_2 = z_3 - \beta_2 fal(e, a_1, \delta) + f + bu \\ \dot{z}_3 = -\beta_3 fal(e, a_2, \delta) \end{cases} \tag{32}$$

where δ, β_1, β_2, β_3 are a group of parameters to be tuned; f is the total disturbance observed by the observer; b is the control input scaling factor. The saturated nonlinear function $fal(e, a, \delta)$ is

$$fal\,(e, a, \delta) = \begin{cases} |e|^a \operatorname{sgn} e, & |e| > \delta, \\ \dfrac{e}{\delta^{1-a}}, & |e| \leq \delta,\ \delta > 0 \end{cases} \tag{33}$$

4. **Simulation and Result Analysis.**

4.1. **Simulation parameters.** According to the mathematical model of the tilt dual-rotor aircraft established according to Equation (18) and the control system block diagram as shown in Figure 3, in order to verify the resistance to wind disturbance and robustness of the aircraft control system in the wind field, a simulation model was constructed in Matlab/Simulink to perform the simulation experiments. The physical parameters of the tilt dual-rotor aircraft are shown in Table 1.

The controller parameters of the inner-ring sliding-mode ADRC control are listed in Table 2. r of TD is an adjustable fast factor, the larger r is, the faster the tracking speed, and the overshoot is more likely to occur; the smaller r is, the longer the tracking process,

TABLE 1. Parameters of the aircraft physical model

Physical quantity/unit	Numerical value	Physical meaning
$m/(\text{kg})$	1.047	Quality
$L/(\text{m})$	0.3	Axial distance
$C_T/(\text{Nm/rad/s})$	0.47	Lift coefficient
$g/(\text{m}\cdot\text{s}^2)$	9.81	Gravitational acceleration
$J_r/(\text{kg}\cdot\text{m}^2)$	$0.5 * 10^{-4}$	Rotor moment of inertia
$J_x/(\text{kg}\cdot\text{m}^2)$	0.04375	x-axis moment of inertia
$J_y/(\text{kg}\cdot\text{m}^2)$	$9.6443 * 10^{-3}$	y-axis moment of inertia
$J_z/(\text{kg}\cdot\text{m}^2)$	0.0124	z-axis moment of inertia

TABLE 2. Parameters of the ADRC controller

	TD	ESO	SMC+NLSEF
Roll angle ϕ	$r = 100$	$\alpha_1 = 0.5$, $\alpha_2 = 0.25$, $b_0 = 1$, $\delta = 0.001$, $\beta_1 = 200$, $\beta_2 = 2000$, $\beta_3 = 20000$	$k_1 = 10$ $k_2 = 7.5$
Pitch angle θ	$r = 100$	$\alpha_1 = 0.5$, $\alpha_2 = 0.25$, $b_0 = 1$, $\delta = 0.001$, $\beta_1 = 200$, $\beta_2 = 2000$, $\beta_3 = 20000$	$k_1 = 10$ $k_2 = 7$
Yaw angle ψ	$r = 100$	$\alpha_1 = 0.5$, $\alpha_2 = 0.25$, $b_0 = 1$, $\delta = 0.001$, $\beta_1 = 100$, $\beta_2 = 900$, $\beta_3 = 5000$	$k_1 = 10$ $k_2 = 8$

and the real-time performance will become worse. The smaller the α_i of ESO is, the faster the tracking speed, but the filtering effect will degrade. β_i is the controller gain and affects the convergence speed, which will not change due to the change of the control object. k_1 and k_2 in SMC+NLSEF have a great impact on the control effect, if they are too large, the system will diverge, and if they are too small, the system will have poor real-time performance.

4.2. **Analysis of simulation results.** Without considering the external disturbances, given the expected position, a comparative experiment was carried out according to the position ring of the designed controller, and the experiment aimed to verify the correctness of the outer ring of the designed controller. By considering the wind field disturbances, given the expected attitude angle, the attitude angle tracking comparative experiment was carried out. The hovering control was realized in the wind field, and finally, the flight trajectory tracking experiment was carried out.

4.2.1. *Position trajectory tracking.* Figure 6 shows the position trajectory tracking curves, in which x_d, y_d, z_d are the expected positions. Compared with the position trajectories in the PID control and the fuzzy adaptive PID control, the sinusoidal signals are added in this control. The initial simulation conditions are $x = 0$ m, $y = 0$ m, $z = 0$ m; the simulation time is 40 s. After adding the ideal signals to the aircraft, in the x direction, PID control achieves the first full tracking in 2.75 s, with the maximum amplitude error of 12.15%; the fuzzy adaptive PID control achieves the first full tracking in 2.13 s, with the maximum amplitude error of 7.3%. The fuzzy adaptive PID control has smaller tracking error and shorter tracking response time. In the y direction, PID control achieves the first full tracking in 2.51 s, with the maximum amplitude error of 12.25%; the fuzzy adaptive PID control achieves the first full tracking in 1.35 s, with the maximum amplitude error of 6.55%. The fuzzy adaptive PID control has smaller tracking error and shorter tracking

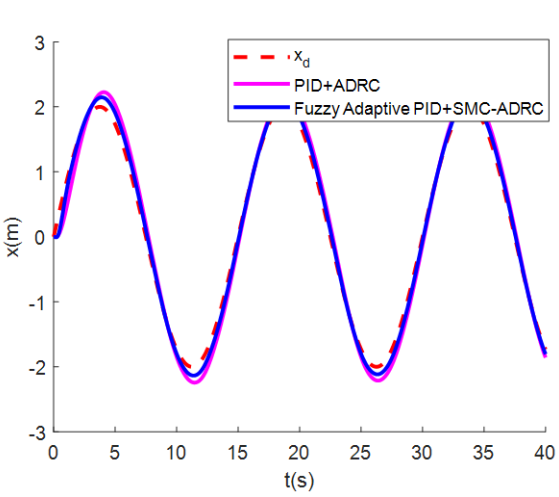

(a) Trajectory tracking in x direction

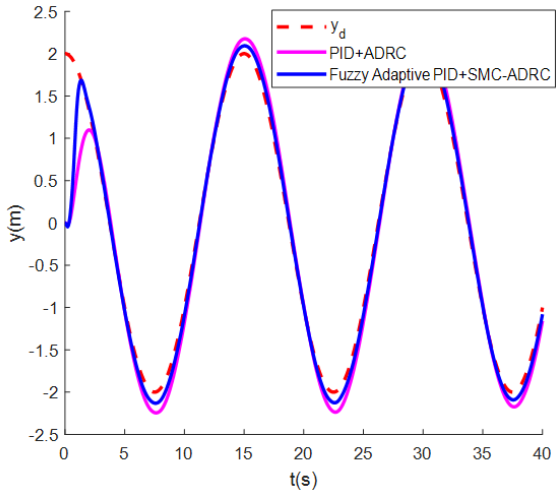

(b) Trajectory tracking in y direction

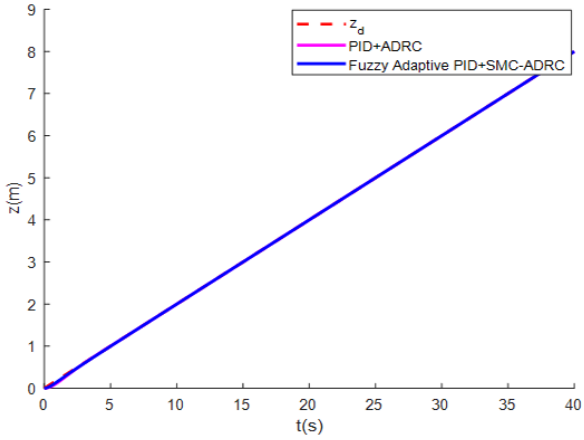

(c) Trajectory tracking in z direction

FIGURE 6. Position trajectory tracking curve

response time. In the z direction, both the fuzzy adaptive PID control and PID control are fast, and both can accurately track the ideal trajectory. According to the simulated comparison curves, the fuzzy adaptive PID controller can provide better position control of the aircraft than the traditional PID control. The fuzzy adaptive PID controller can better track the expected position trajectory. This controller has a small error and better steady-state performances and can better follow the signal, which effectively solves the problem that the parameters cannot be tuned online in the PID control.

4.2.2. *Attitude trajectory tracking under wind disturbances.* In this simulation, the internal coupling was removed, but the wind field disturbance was retained. Figure 7 shows the comparison between the real values and the estimated values of the turbulent wind field disturbances by the ESO in the attitude loop roll channel ϕ, pitch channel θ, and yaw channel ψ. The simulation time was set as 40 s; the turbulence flow wind field parameter was $u_{20} = 10$ m/s; the flight height was 20 m; the wind field parameter scale factors: $L_u = 143.589$ m, $L_v = 71.794$ m, $L_w = 10$ m; the wind field intensities: $\sigma_u = 1.930$ m/s, $\sigma_v = 3.722$ m/s, $\sigma_w = 1$ m/s. The simulation results show that the observation values of the ESO can accurately track the actual values, and the actual values of the wind field disturbances can be well estimated and tracked.

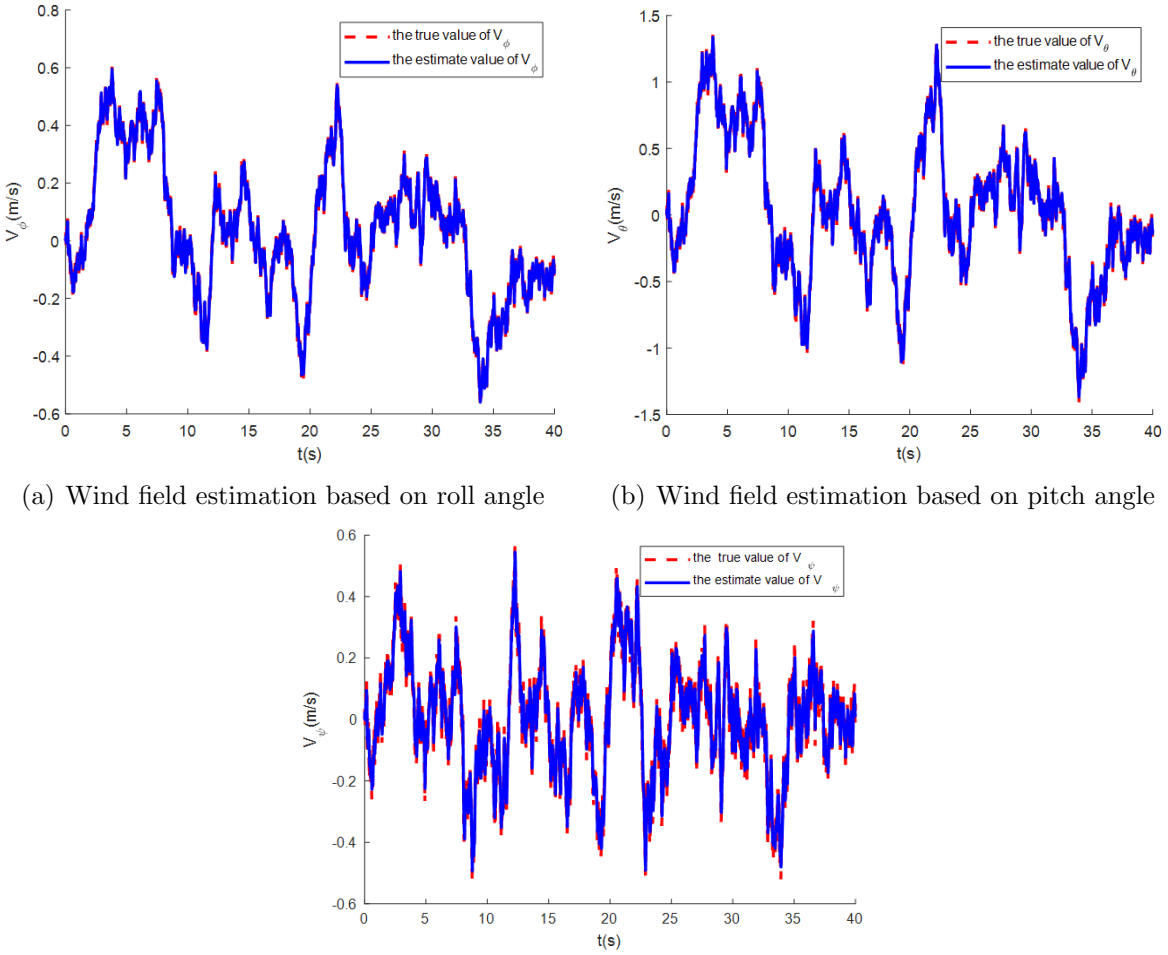

(a) Wind field estimation based on roll angle

(b) Wind field estimation based on pitch angle

(c) Wind field estimation based on yaw angle

FIGURE 7. Wind field disturbance estimation of attitude ring

Figure 8 shows the trajectory tracking by the attitude ring under wind disturbances. ϕ_d, θ_d and ψ_d are the expected values of the roll, pitch, and yaw attitudes, which are compared with the ADRC attitude trajectory and the sliding-mode ADRC attitude trajectory. The simulation time was 40 s; the initial conditions of the attitude control simulation: $\phi = 0$ rad, $\theta = 0$ rad, $\psi = 0$ rad; the turbulent wind field disturbance signals w_2, w_3, w_4 were introduced to the three channels of pitch, roll and yaw, respectively, and the attitude angle trajectory tracking experiment was carried out under the wind field disturbances. The active disturbance rejection overshoot of roll angle ϕ is -48.74%, the response time is 1.62 s, and the maximum steady-state tracking error is 1.59%; the sliding-mode active disturbance rejection overshoot is -12.5%, the response time is 1.07 s, the maximum steady-state tracking error is 1.07%, and the sliding-mode active disturbance rejection tracking trajectory is obviously superior to the active disturbance rejection tracking trajectory. The active disturbance rejection overshoot of pitch angle θ is -23.68%, the response time is 0.4 s, and the maximum steady-state tracking error is 9.8%; the sliding-mode active disturbance rejection overshoot is -10.47%, the response time is 0.385 s, the maximum steady-state tracking error is 1.67%, and the sliding-mode active disturbance rejection tracking trajectory is significantly superior to the active disturbance rejection tracking trajectory. The active disturbance rejection overshoot of pitch angle θ is -23.68%, the

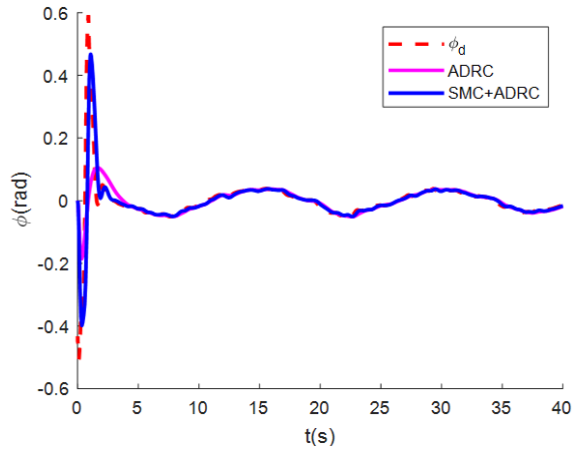

(a) Trajectory tracking of the roll angle

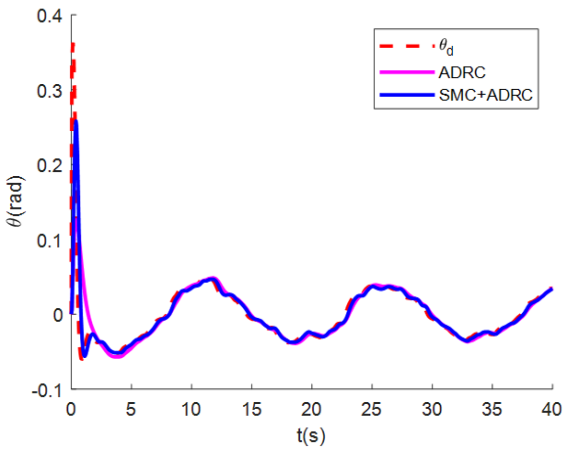

(b) Trajectory tracking of the pitch angle

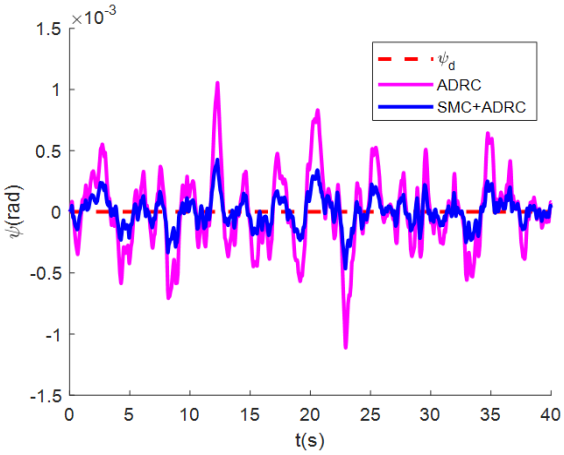

(c) Trajectory tracking of the yaw angle

FIGURE 8. Attitude trajectory tracking curves under wind filed disturbances

response time is 0.4 s, and the maximum steady-state tracking error is 9.8%; the sliding-mode active disturbance rejection overshoot is −10.47%, the response time is 0.385 s, the maximum steady-state tracking error is 1.67%, and the sliding-mode active disturbance rejection tracking trajectory is significantly superior to the active disturbance rejection tracking trajectory. The maximum deviation of the yaw angle ψ ADRC is 1.112×10^{-3}, the maximum deviation of the sliding-mode ADRC is 0.4654×10^{-3}, the average value of the ADRC in the time range is −5.947E-07, and the average value of the sliding-mode ADRC in the time range is −1.317E-07. Obviously, the sliding mode ADRC is superior to the ADRC. It can be seen that the given value can be well tracked under the wind field disturbances, indicating that the designed controller can effectively suppress the wind field disturbance, and effectively control the attitude system of the aircraft with strong coupling.

4.2.3. *Hovering control of aircraft.* The hovering trajectory of the aircraft under the wind field disturbances is shown in Figure 9. The initial position was set to $[0, 0, 0]$, and the target hovering position was set to $[8, 8, 8]$ for the reference trajectory. Under the ideal hovering and flight trajectory, the hovering trajectory of the designed algorithm was 2 s faster than the PID-ADRC hovering trajectory, and the aircraft could stably hover at $[8, 8, 8]$, and achieve stable hovering and flight. The uncertain external disturbances from

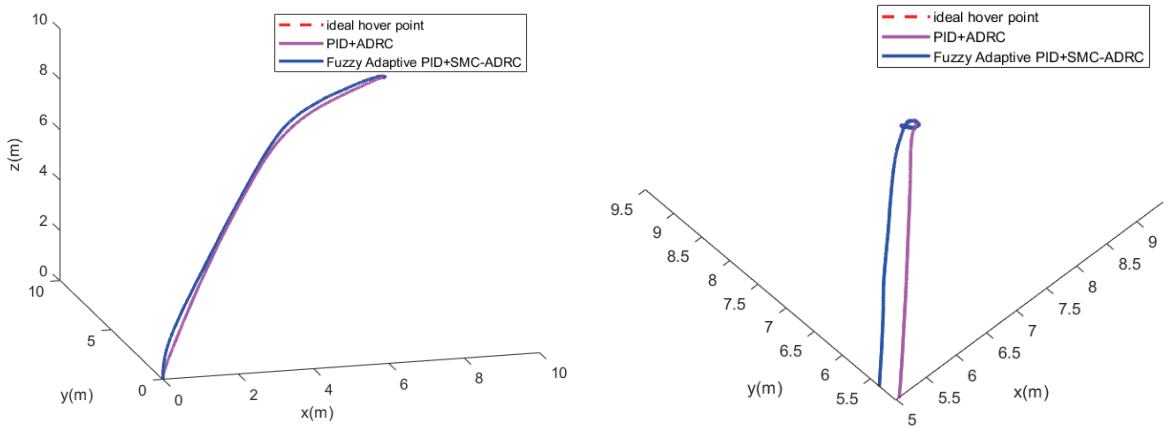

(a) 3D hovering control tracking curve (b) Top view of the 3D hovering tracking curve

FIGURE 9. Hovering control curve

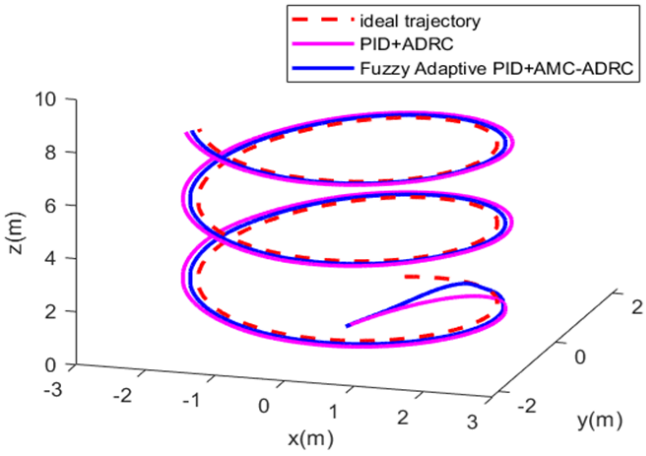

FIGURE 10. Tracking of flight trajectory

the wind field can be estimated and suppressed with our algorithm, which can not only increase the position control accuracy, but also improve the stability of the aircraft attitude.

4.2.4. *Flight trajectory tracking control.* Figure 10 shows the 3D flight trajectory tracking of the aircraft, in which the expected flight trajectory, the flight trajectory obtained by combining the fuzzy adaptive PID control and sliding-mode ADRC, and the flight trajectory obtained by combining the PID control and ADRC are compared. Assuming the initial state of the aircraft was static, the initial position was set to $(\ 0 \quad 0 \quad 0\ )^T$, and the initial attitude was set to $(\ 0 \quad 0 \quad 0\ )^T$. The yaw angle was set to 0°. The expected trajectory is

$$\begin{cases} x_d = 2\sin\left(\dfrac{2}{15}\pi t\right) \\ y_d = 2\cos\left(\dfrac{2}{15}\pi t\right) \\ z_d = 0.2t \end{cases} \tag{34}$$

The simulation time was 40 s, the initial height was 0 m, and the total height was 10 m. It can be seen from the figure that the flight trajectory obtained by combining the PID

control and ADRC shows the maximum offset distance of 0.24 m, and the maximum offset rate of 12% on the x-axis; the maximum offset distance on y-axis is 0.174 m, and the maximum offset rate is 8.7%. It also presents a deviation of 2 s from the ideal trajectory, which also demonstrates certain deviation during the flight. In comparison, the control strategy combining the fuzzy adaptive PID control and the sliding-mode ADRC designed in our work shows the maximum offset distance of 0.141 m, and the maximum offset rate of 7.05% on the x-axis; the maximum offset distance on y-axis is 0.13 m, and the maximum offset rate is 6.5%. It could quickly track the expected trajectory with relatively small deviation, and a good flight tracking state was maintained throughout the whole process. Therefore, it proves the effectiveness of the controller designed in this paper.

5. **Conclusion.** To address the problems of parameter uncertainty and susceptibility to disturbances from the wind field, this paper proposes a control strategy combining the fuzzy adaptive PID and sliding-mode active disturbance rejection control. Our work can be summarized as follows.

1) The aircraft model under wind disturbance is established. The position ring combines fuzzy control with PID control to realize the online tuning of controller parameters; the attitude inner ring combines the sliding-mode control and the active disturbance rejection control. The expanded state observer is used to estimate the wind disturbance to the aircraft and compensate the wind disturbance in real time.

2) The simulation experiments were performed to verify the effectiveness of position ring and attitude ring controller, and their tracking performances and the estimation and compensation of the wind field are verified. The hovering control and 3D trajectory flight tracking control are realized in the wind field.

REFERENCES

[1] B. Nie, H. Ma and J. Wang, Study on actualities and critical technologies of micro quadrotor, *Electronics Optics & Control*, no.6, pp.113-117, 2007.

[2] R. Zhang, Q. Quan and K. Y. Cai, Attitude control of a quadrotor aircraft subject to a class of time-varying disturbances, *IET Control Theory Applications*, vol.5, no.9, pp.1140-1146, 2011.

[3] X. Guo, Q. Shao, F. Yang, Y. Li and D. Wang, Using UAV remote sensing for a population census of blue sheep in Maduo County, source region of the Yelloe River, *Journal of Natural Resources*, vol.34, no.5, pp.1054-1065, 2019.

[4] Y. More and A. Leonessa, Direct adaptive tracking control of quadrotor aerial vehicles, *Florida Conference on Recent Advances in Robotics*, Miami, FL, USA, pp.1-6, 2006.

[5] J. Zhao, *Research on Control Method and Controller Design for Micro Quadrotor Aricraft*, Master Thesis, Liaoning University of Technology, 2016.

[6] T. Dierks and S. Jagannathan, Neural network control of quadrotor UAV formations, *American Control Conference*, St.Louis, MO, USA, pp.2990-2996, 2009.

[7] R. Kurokawa, N. Kawaguchi, T. Sato and R. Vilanova, Data-driven regulator PID control using a model-reference robust tuning method, *International Journal of Innovative Computing, Information and Control*, vol.18, no.1, pp.1-13, 2022.

[8] Y. Shao, L. Liu, X. Cao et al., Research status and key technologies of tilt-rotor UAVs, *Tactical Missile Technology*, no.1, pp.12-20, 2022.

[9] R. T. Rysdyk and A. J. Calise, Adaptive model inversion flight control for tilt-rotor aircraft, *Journal of Guidance Control & Dynamics*, vol.22, no.3, pp.402-407, 2012.

[10] K. Masuda and K. Uchiyama, Robust control for quad tilt-wing UAV, *Mechatronics*, vol.22, pp.723-745, 2012.

[11] Y. Qu, Z. Xing, D. Yuan et al., Wind field estimation based on position and attitude information of quadrotor in hover, *Journal of Northwestern Polytechnical University*, vol.34, no.4, pp.684-690, 2016.

[12] Y. Zhao and Y. Wang, Research on anti-disturbance for quadrotor aircraft in wind field, *Mechanical Science and Technology for Aerospace Engineering*, vol.38, no.4, pp.530-537, 2019.

[13] J. Liang, Y. Shi and X. Zhou, Adaptive inversion sliding mode control of a quad-rotor subject to turbulent wind disturbances, *Information & Communications*, no.2, pp.85-88, 2019.
[14] L. Tang, W. Lu, F. Gong et al., Double power reaching law for sliding mode control of the quadrotor UAV based on wind disturbance observation, *Flight Dynamics*, vol.37, no.6, pp.27-33+39, 2019.
[15] N. El Gmili, M. Mjahed, A. El Kari and H. Ayad, Particle swarm optimization based proportional-derivative parameters for unmanned tilt-rotor flight control and trajectory tracking, *Automatika*, vol.61, no.2, pp.189-206, 2020.

Author Biography

Liben Yang received the Ph.D. degree in Control Science and Engineering from Northwestern Polytechnical University.

Dr. Yang is currently a full-time associate professor at the School of Automation and Electrical Engineering, Lanzhou Jiaotong University. His research interests include autonomous control and autonomous repair control of underactuated aircraft.

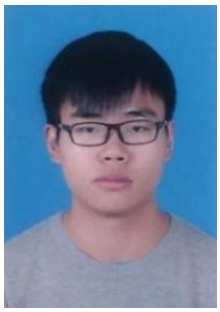

Yumin Tang is currently studying for a master's degree in transportation in the School of Automation and Electrical Engineering of Lanzhou Jiaotong University. His main research interests include aircraft control and underactuated control.

Wenjun Wei received a doctorate in engineering from Lanzhou Jiaotong University.

Prof. Wei is currently a full-time professor at the School of Automation and Electrical Engineering, Lanzhou Jiaotong University. He has published more than 20 academic papers, which have been indexed by EI, ISTP and many domestic core journals. His research interests include fault diagnosis of dynamic systems, and intelligent control theory and application.